Perpendicular Fiber Tracking for Neural Fiber Bundle Analysis using Diffusion MRI

S. Ray

Department of Biomedical Engineering,
University of Florida,
Gainesville, FL 32611, USA
E-mail: siddharthray@ufl.edu

W. O'Dell

Department of Radiation Oncology,
University of Florida,
Gainesville, FL 32601, USA
E-mail: wodell@ufl.edu

Angelos Barmpoutis*

Digital Worlds Institute,
University of Florida,
Gainesville, FL 32611, USA
Fax: 1-352-294-2030
E-mail: angelbar@ufl.edu
*Corresponding author

Abstract: Information on the directionality and structure of axonal fibers in neural tissue can be obtained by analyzing Diffusion-Weighted MRI datasets. Several fiber tracking algorithms have been presented in literature that trace the underlying field of principal orientations of water diffusion, which correspond to the local primary eigenvectors of the diffusion tensor field. However, the majority of the existing techniques ignore the secondary and tertiary orientations of diffusion, which contain significant information on the local patterns of diffusion. In this paper we introduce the idea of perpendicular fiber tracking and we present a novel dynamic programming method that traces surfaces, which are locally perpendicular to the axonal fibers. This is achieved by using a cost function, with geometric and fiber orientation constraints, that is evaluated dynamically for every voxel in the image domain starting from a given seed point. The proposed method is tested using synthetic and real DW-MRI datasets. The results conclusively demonstrate the accuracy and effectiveness of our method.

Keywords: diffusion-weighted MRI; diffusion tensor imaging; fiber tracking; DTI tractography.

Reference to this paper should be made as follows: Ray, S., O'Dell, W. and Barmpoutis, A. (2012) 'Perpendicular Fiber Tracking for Neural Fiber Bundle Analysis using Diffusion MRI', *Int. J. Bioinformatics and Research Applications*, Vol. x, Nos. x, pp.1–15.

Biographical notes: S. Ray received his BE from Shri Govindram Seksaria Institue of Technology and Science, MS in Biomedical Engineering from Louisiana Tech University in 2011 and MS in Biomedical Engineering from the University of Florida in 2012. His areas of interest are medical image processing, diffusion tensor imaging, tractography.

W. O'Dell received his BS in Applied and Engineering Physics from Cornell University in 1986 and PhD in Biomedical Engineeing from Johns Hopkins University in 1995. He is presently working as an Assistant Professor in the Department of Radiation Oncology and he is also Affilate Professor in the Department of Biomedical Engineering, University of Florida. His research interest includes medical image processing, 3D motion tracking and motion correction, image registration, radiotherapy and radiosurgery.

Angelos Barmpoutis received his BS in Computer Science from Aristotle University of Thessaloniki in 2003, MS in Electronics and Electrical Engineering from the University of Glasgow in 2004, and PhD in Computer Engineering from the University of Florida in

2009. He is presently an Assistant Professor at the Digital Worlds Institute and Affiliate Professor at the Computer and Information Science and Engineering Department at the University of Florida. His research interests lie in the areas of machine vision and applications, virtual reality in medicine, human motion capture and analysis, biomedical image processing and visualization, and facial recognition and expression analysis.

1 Introduction

Diffusion Tensor Magnetic Resonance Imaging (9) has recently gained much attention for analyzing the diffusivity patterns in neural tissues and visualizing the reconstructed neural fiber tracts (11). In Diffusion Tensor Imaging (DTI), the diffusion coefficient is a 3×3 symmetric positive semi-definite matrix. The largest eigenvector of the diffusion tensor is assumed to be oriented parallel to the local fiber tracts, which can be reconstructed in a brain dataset by following paths in the estimated eigenvector field. The characteristic features of the traced neural fiber networks, such as structure, topology, and connectivity, can serve as biomarkers for various *dementias* and brain diseases, and can be used in various clinical applications.

The topic of tractography has been significantly studied in the past decade, and several techniques have been proposed using either deterministic or probabilistic formulations (11; 22; 13; 29; 20; 16; 12; 14). A technical review of the principles and strategies of fiber tracking can be found in (23). In deterministic or streamline tractography, there is a continuous agreement between connected points along the fiber bundle. Tracking starts at a seed point and follows a favored direction for a pre-defined small step size and it continues following the corresponding fiber directions along the path. The fiber tracking method developed by Basser et al. (11) is an illustrative example of deterministic tractography. This technique was extended by Mori et al. (22) introducing fiber assignment by continuous tracking. The computational cost of deterministic tractography is low and output tracts are easy to interpret. However, as calculations are made on local scale, error is accumulated along the tracts as one traces farther from the seed location.

In probabilistic tractography (12), fiber tracts are computed by using a diffusion propagation model in the form of a field of spherical functions, instead of relying directly on the vector field of the principal orientations of diffusion. The fiber tracking is done repeatedly, each time in a slightly different direction. The set of all the different paths is then collectively analyzed to compute the most highly probable direction. This method gives a more detailed picture of fiber connectivity in brain and it is more robust in complex intra-voxel fiber configuration. Compared to deterministic tractography this approach is computationally costly and the outcome connectivity maps are more difficult to interpret.

In addition, other approaches have been introduced that combine both the aforementioned tractography strategies. In (13) the presented Split and Merge Tractography technique tracks all the fiber tracts inside the area of interest while minimizing the total energy. Although using short fiber tracts improves significantly the accuracy in fiber tracking compared to the deterministic approaches, the computational cost is still high. More recently, global energy minimization algorithms have been introduced for short fiber clustering (29; 20; 16). In these works, short fiber tracts are randomly generated and are allowed to move, rotate, and assemble with other fibers to minimize internal and external energies.

However, the process of fiber tracking in general ignores the secondary and tertiary orientations of diffusion, which contain significant information on local patterns of diffusion. In this paper, we introduce the idea of perpendicular fiber tracking and we present a novel dynamic programming method that traces surfaces that are locally perpendicular to the axonal fibers. The tracing of a fiber section is in general a more complex task compared to the traditional single dimensional fiber tracking, since the former requires simultaneous tracking on both secondary and tertiary diffusion directions while maintaining continuity constraints of the estimated surface. In the proposed algorithm we achive this by introducing two cost functions that impose geometric and fiber constraints to the obtained solution. The geometric cost controls the connectivity and continuity of the traced surface, while the fiber cost enforces the normal vectors on every point of the computed surface to be parallel to the underlying fiber orientation.

One of the goals of this work is to apply the proposed fiber tracking method on a practical clinical application for fiber bundle analysis and quantitative comparison of the differences in their structure and topology. The proposed algorithm performs tracing of fiber bundle sections, perpendicular to local dominant fiber orientation, and computes their area and average curvature along a fiber bundle. To the best of our knowledge there is no prior literature on perpendicular fiber tracking and thus requires a thorough validation. As the ground truth geometry of real brain datasets is not known, a synthetic dataset of a pre-defined structure with known fiber geometry was constructed and used to test the accuracy of the algorithm.

The contributions in this paper are threefold:

- We introduce the idea of perpendicular fiber tracking, which is a process for computing a surface which is perpendicular to the underlying local fiber orientations, starting from a given seed point.
- We present a novel and computationally efficient algorithm for perpendicular fiber tracking using dynamic programming.
- Furthermore, we present a novel algorithm for fiber bundle analysis with applications in fiber bundle segmentation and statistical analysis of its features, such as surface area and average curvature.

The key advantage of the proposed perpendicular fiber tracking method is that reconstructs structures larger than the size of one voxel in typical DW-MRI resolutions. In contrast, the traditional fiber tracking algorithms track axonal fibers, which are structures with diameter significantly smaller than one voxel. Therefore, data analysis based on fiber bundles is expected to be more robust than a corresponding analysis based on single fibers.

The proposed algorithm for perpendicular fiber tracking can be perceived as the extension in two dimensions of probabilistic tractography methods. Our technique can use any mathematical model of diffusion for computing a cost map that assigns large penalties to the voxels that do not belong to our solution. Such mathematica models of diffusion may include diffusion tensors, high-order tensors, orientation distribution functions, fiber orientations distributions and other models discussed in Sec. 2.

We demonstrate the proposed algorithm using synthetic and real DW-MRI datasets from rat hippoxampus. We test quantitatively the accuracy of the obtained resultys and their robustness with respect to the input parameters in simulated datasets with known underlying fiber geometry. Several examples of different known fiber bundles in the area of hippocampus are presented in the form of cost maps, tridimensional surfaces, segmented fiber bundles, and plots of features along the traced fiber bundles.

The rest of the article is organized as follows: In Sec. 2 we review several mathematical models for representing the underlying distinct fiber orientations within a single voxel of a DW-MRI dataset. In Sec. 3 we present the perpendiculat fiber tracking algorithms and we introduce several cost functions in Sec. 3.1 (fiber cost), 3.2 (geometric cost), and 3.3 (joint cost) that are employed by our algorithm. In Sec. 4 we present an application of the perpendicular fiber tracking method for fiber bundle analysis. Sec. 5 is further organized into two subsections that present the experimental results obtrained by using synthetic and real dataset. Finally, in Sec. 6 we discuss further the details of our algorithms and we conclude.

2 Mathematical models of diffusion patterns

A diffusion MRI dataset consists of several images $S_1, S_2, \cdots S_N$ of the same subject acquired usually in one scanning session (to avoid image registration steps). Each image S_i is associated with a diffusion sensitizing gradient orientation ($\mathbf{g}_i \in S_2$) and a diffusion weighting factor ($b_i \in \mathbb{R}_+$). The pattern of diffusion within each voxel of a DW-MRI dataset can be studied in the form of a continuous function $S(b, \mathbf{g})$ that is estimated after fitting a parametric model to the aquired signals $S(b_i, \mathbf{g}_i) = S_i \ \forall \ i = 1 \cdots N$.

The DW-MRI signal attenuation has been modeled by Stejskal and Tanner (32) as follows:

$$S/S_0 = e^{-bd} \tag{1}$$

where S_0 correspond to the signal without diffusion-weighting, and d is the unknown average diffusion coefficient (ADC) that is estimated after fitting the data to Eq.1.

If the number of distinct diffusion sensitizing gradient orientations is at least 6, it has been shown (8; 10) that the diffusion coefficient in Eq. 1 can be extended to a spherical function $d(\mathbf{g})$:

$$S(b, \mathbf{g}) = S_0 e^{-bd(\mathbf{g})} \tag{2}$$

where $d(\mathbf{g})$ is a second-order homogeneous polynomial in three variables that can be written in the form of a 2^{nd}-order tensor $d(\mathbf{g}) = \mathbf{g}^T \mathbf{D} \mathbf{g}$. The 3×3 diffusion tensor matrix $\mathbf{D}$ is symmetric positive definite, since negative diffusion values do not have valid physical meaning. The advantage of the tensor model in Eq.2 over the model in Eq.1 is that information on the directionality of diffusion can be estimated by calculating the eigenvectors of $\mathbf{D}$. The maximum orientation of diffusion has been widely used in tractography and other DW-MRI signal processing algorithms.

Following similar reasoning, the model in Eq.2 has been extended using higher-order diffusion tensors (HOT) (25; 4) $d(\mathbf{g}) = \sum_{i+j+k=n} g_1^i g_2^j g_3^k D_{i,j,k}$, where n corresponds to the order of the tensor model. The number of unknown coefficients increases by the order of the model as follows $\frac{(n+2)(n+1)}{2}$, which corresponds to the minimum number of DW-MRI images required.

At this point we should note that all the aforementioned models use a linear-exponential signal attenuation with respect to b. This relationship can be extended using a quadratic-exponential signal decay by adding the kurtosis component of diffusion (DKI) (18; 26) in Eq.2 as follows:

$$S(b, \mathbf{g}) = S_0 e^{-bd(\mathbf{g}) + \frac{b^2 \bar{d}^2}{6} w(\mathbf{g})} \tag{3}$$

where $\mathbf{w}(\mathbf{g})$ is a 4^{th}-order homogeneous polynomial in three variables, and $\bar{d} = \int_{S_2} d(\mathbf{g}) d\mathbf{g} / 4\pi$ is the average value of the 2^{nd}-order component of the diffusion $d(\mathbf{g})$. This model requires data acquisition using at least two b values, forming two acquisition shells. In the case that a

single b value is employed in the acquisition scheme, the model in Eq.3 is identical to the higher order diffusion tensor model (order $n = 4$) (7).

Although the HOT and DKI models can approximate complex patterns of diffusion, such as crossing fibers, they cannot be used directly in tractography because the orientations of their maxima do not correspond to the underlying fiber orientations. Instead, the orientations of the maxima of the diffusion propagator should be estimated using the 3-dimensional inverse Fourier transform:

$$S(\mathbf{q})/S_0 = \int P(\mathbf{r}) e^{2\pi i \mathbf{q}\cdot\mathbf{r}} d\mathbf{r} \tag{4}$$

where $P(\mathbf{r})$ is the diffusion propagator and $\mathbf{r}$ is a displacement vector in the 3D space. The vector $\mathbf{q}$ is a 3D vector with the same orientation as the gradient $\mathbf{g}$ in Eq. 3 and its magnitude is proportional to diffusion-weighting b. The unknown diffusion propagaror $P(\mathbf{r})$ can be estimated from a given model of the signal using the Fourier transform, either by approximating numerically the integral or by using Orientation Distribution function model (ODF) that approximates the diffusion propagator (34; 2; 17; 15; 1).

Another model that can be used in fiber tractography is the spherical deconvolution models (33; 27; 28; 21; 19):

$$S(b, \mathbf{g}) = \int_{S_2} w(\mathbf{r}) B(b, \mathbf{g}, \mathbf{r}) d\mathbf{r} \tag{5}$$

where the unknown function $w(\mathbf{r})$ is the so called Fiber orientation distribution (FOD), $B(b, \mathbf{g}, \mathbf{r})$ is a given model of a single fiber with orientation $\mathbf{r}$. Note that the vector $\mathbf{r}$ in Eq. 5 is a unit vector, compared to the vector in Eq.4, which belongs to $\mathbb{R}^3$.

The models that we reviewed in this section approximate the diffusion pattern within one voxel of a DW-MRI dataset, and can be used by probabilistic and deterministic fiber tracking algorithms that infer the diffusion patterns along the major orientations of diffusion. In the next section we propose a novel perpendicular fiber tracking algorithm that can employ any of the aforementioned models in order to estimate sections of fiber bundles, which are perpendicullar to the local fiber orientations.

3 Perpendicular Fiber Tracking

In this section we introduce the idea of perpendicular fiber tracking and we present an algorithmic implementation using dynamic programming. The algorithm uses as its input a field of the distinct orientations of diffusion that can be provided by any of the models in Sec. 2. Perpendicular fiber tracking is the process of estimating a 2D-surface in the 3D image domain of a DW-MRI dataset that passes through a given seed point and it is locally perpendicular to the underlying fiber orientation (or one of the underlying fiber orientations in the case of multi-fiber diffusion profiles). This definition includes three key geometric constraints:

- Fixed point constraint: The surface should pass through a given seed point.
- Connectivity constraint: The result should form a connected surface.
- Fiber contraint: The normal vector on each point of the surface should be parallel to the most coherent local fiber orientation.

In addition to the above conditions, a continuity constraint can also be added to the definition of our problem, in order to enforce estimation of continuous surfaces. A surface that satisfies all the above constraints can be estimated using various algorithms, such as optimization techniques that minimize an energy function, which implements the aforementioned constraints.

In order to develop an algorithmic solution with minimal computational complexity, we solve the problem by estimating a cost map instead of a parametric surface using dynamic programming. The cost map represents the probability that a point belongs to the solution surface. A parametric surface can be easily extracted from the cost map, if needed, using iterative contour estimation. Dynamic programming has been used in various applications in computer vision, including image processing and interactive segmentation (24).

Starting from a given seed voxel with zero cost, our dynamic programming implementation keeps a sorted list of all the exterior neighboring voxels and expands the solution towards that neighboring voxel with the smallest cumulative cost. The sorting of the list of active voxels, is obviously with respect to the cumulative cost. The complexity of adding a new voxel to the sorted list is known to be $O(\log n)$. The iterative algorithm stops when all voxels in the image domain have an assigned cost, which brings the overall complexity of the algorithm to $O(n \log n)$. However, it can be easily observed that the voxels outside the solution surface have significantly larger cost and therefore the iterative process can be safely terminated when the smallest cumulative cost in the active list exceeds a user-defined threshold before assigning cost values to voxels outside of the region of interest (i.e. solutions surface).

At this point we would like to emphasize that the cumulative cost at a voxel is the summation of the cost for transitioning from the seed point to that particular voxel by following the smallest cost path. In order to reconstruct the shortest paths between any voxel and the given seed point, our algorithm keeps for each voxel in the solution set, not only its cumulative cost, but also the voxel identity of its hierarchical father. Starting from any voxel, one can transition to its hierarchical father, grandfather, etc. until the seed point is reached.

3.1 Fiber Cost

The cost map estimation process is driven by a cost function that consists of 2 terms: 1) a fiber orientation cost and 2) a geometric cost. The fiber cost ensures that each point on the estimated surface is perpendicular to the local fiber orientation. It measures the degree of perpendicularity between the fiber orientation at the candidate voxel $\mathbf{v}$ and the local orientation of the estimated surface expressed as the vector from the candidate voxel to its hierarchical father voxel $father(\mathbf{v})$. The fiber cost can be expressed as

$$Cost_f(\mathbf{v}) = \left| \frac{\mathbf{v} - father(\mathbf{v})}{\|\mathbf{v} - father(\mathbf{v})\|} \cdot fiber(\mathbf{v}) \right| \quad (6)$$

where $\mathbf{v}$ is the voxel location ($\mathbf{v} \in \mathbb{N}^3$), $father(\mathbf{v}) \in \mathbb{N}^3$ is the voxel location of the hierarchical father of $\mathbf{v}$, and $fiber(\mathbf{v})$ is the underlying fiber orientation at voxel $\mathbf{v}$, ($fiber(\mathbf{v}) \in S_2$, i.e. a unit vector). The norm in Eq. 6 is the Euclidean distance.

As it was discussed in Sec. 2, the underlying fiber orientation at a given voxel can be estimated by various mathematical models, some of which have the ability to perform multi-fiber reconstruction, and hence provide more than one fiber orientations in the case of multi-fiber crossing within a voxel of a DW-MRI dataset. In the case of the Diffusion Tensor model (Eq. 2), $fiber(\mathbf{v})$ is given by the primary eigen vector of the matrix $\mathbf{D}$. Multi-fiber reconstruction models, such as HOT, DKI, ODF, FOD, and others may compute more than one fiber orientations given by $fiber_i(\mathbf{v})$ $i = 1..N$, where N is the number of reconstructed fibers, which is typically 1 for a single fiber, and 2 or 3, for 2-fiber or 3-fiber crossings respectively. In this case Eq. 6 can be generalized as

$$Cost_f(\mathbf{v}) = \min_i \left| \frac{\mathbf{v} - father(\mathbf{v})}{\|\mathbf{v} - father(\mathbf{v})\|} \cdot fiber_i(\mathbf{v}) \right| \quad (7)$$

which computes the cost that corresponds to the most coherent fiber orientation, i.e. the fiber that is more perpendicular to the estimated surface.

3.2 Geometric Cost

The geometric cost ensures the continuity of the estimated surface within a fiber bundle. This definition makes use of the fact that a fiber bundle corresponds to a smoothly varying field of fiber orientations. Under this assumption, adjacent voxels on the solution surface should correspond to similarly oriented underlying fibers. In our implementation the geometric cost measures the degree of parallelism between the fiber orientation at the candidate voxel $\mathbf{v}$ and the fiber orientation at its hierarchical father voxel $father(\mathbf{v})$. The geometric cost can be expressed as

$$Cost_g(\mathbf{v}) = 1 - |fiber(\mathbf{v}) \cdot fiber(father(\mathbf{v}))| \quad (8)$$

where $\mathbf{v}$ and $father(\mathbf{v})$ are defined as in Eq. 6. In the case of employing a multi-fiber reconstruction model for computing the underlying fiber orientations, Eq. 8 can be extended as follows:

$$Cost_g(\mathbf{v}) = \min_i (1 - |fiber_i(\mathbf{v}) \cdot fiber(father(\mathbf{v}))|) \quad (9)$$

where the index i runs for all fiber orientations in the candidate voxel $\mathbf{v}$. There fiber orientation of the father of $\mathbf{v}$ corresponds to that particular orientation that gave the smallest cost when $father(\mathbf{v})$ was a candidate voxel. In multi-fiber reconstruction case, the chosen fiber orientation should be stored for all the voxels in the solution space, along with their cost value and father's index.

3.3 Joint Cost

The role of the joint cost function is to ensure that both fiber and geometric conditions are satisfied simultaneously. In a discrete binary case (Boolean case) such a function would correspond to the logical 'AND' function. In a continuous implementation (fuzzy logic cases), the logical 'AND' function is represented by multiplication of values in the interval [0-1], where a zero value represents the negative Boolean state (i.e. false state), and a unit value represents the positive Boolean state (i.e. true state). In our particular case the positive (desirable) state corresponds to low cost, (i.e. low cost is desired), which is represented by the logical function $1 - Cost(\mathbf{v})$. Therefore, the joint cost function can be written in the following fuzzy-logic form:

$$Cost(\mathbf{v}) = 1 - (1 - Cost_f(\mathbf{v}))(1 - Cost_g(\mathbf{v})) \quad (10)$$

where $Cost_f(\mathbf{v})$ and $Cost_g(\mathbf{v})$ are given by Eq.6 and Eq.8 respectively. The joint cost function given by Eq.10 can be used along with single fiber orientation vector fields, such as those computed by the DTI model (Eq. 2).

The joint cost function that should be used along with multi-fiber recostruction models generalizes Eq.10 by 'merging' the min functions in Eqs.7 and 9 as follows:

$$Cost(\mathbf{v}) = \min_i (1 - (1 - Cost_f(\mathbf{v}))(1 - Cost_g(\mathbf{v}))) \quad (11)$$

where the index i runs for all reconstructed fiber orientations in the candidate voxel $\mathbf{v}$, and the functions $Cost_f(\mathbf{v})$ and $Cost_g(\mathbf{v})$ are evaluated by the formulas in Eqs. 6 and 8 respectivelly using $fiber_i(\mathbf{v})$ instead of $fiber(\mathbf{v})$. As a result, the total cost function selects that particular fiber orientation in the candidate voxel $\mathbf{v}$ that yields the smallest joint fiber and geometric cost. In practice, the voxels that belong to our solution surface will have smaller costs assigned to them than the voxels outside the perpendicular fiber section.

In the next section we employ the joint cost function presented here in order to construct a 3D cost map using dynamic programming.

3.4 Computation of the 3D cost map

The dynamic programming algorithm for perpendicular fiber tracking was formulated as a graph search for

a minimum cost map. Graph search based dynamic programming algorithms have been used in many applications in computer vision and interactive image segmentation (24). Our proposed algorithm requires a seed voxel and a field of fiber orientations as its input data. The result (i.e. the cost map) is computed in the form of a three dimensional matrix $\mathbf{C}$. The algorithm is summarized below.

Algorithm *Perpendicular_Fiber_Tracking*

Input: A seed voxel location $\mathbf{s}$. A field of fiber (or multi-fiber) orientations.
Output: The cost map $\mathbf{C}$ (a 3D matrix).

1 Initialize: $L \leftarrow \mathbf{s}$; $\mathbf{C} \leftarrow \infty$;

2 If $L = \emptyset$ stop algorithm and return $\mathbf{C}$, otherwise continue.

3 Remove the voxel $\mathbf{m}$ from L with the minimum cost $\mathbf{C}(\mathbf{m})$.

4 For all voxels $\mathbf{v}$ with $\mathbf{C}(\mathbf{v}) = \infty$ in the neighborhood of $\mathbf{m}$ do: $L \leftarrow L \cup \mathbf{v}$; $father(\mathbf{v}) \leftarrow \mathbf{m}$; $\mathbf{C}(\mathbf{v}) \leftarrow Cost(\mathbf{v})$;

5 Go to step 2.

End *Perpendicular_Fiber_Tracking*

For the calculation of the cost in step 4 of the algorithm, the joint cost function is employed (Sec. 3.3). Note that in the calculations of the cost function, the voxel $\mathbf{m}$ is used as the the hierarchical father of the candidate voxel $\mathbf{v}$. Depending on the type of the input field of fiber orientations, the DTI or the multi-fiber version of the joint cost function can be used respectively (Eqs. 10 and 11).

The main body of the proposed algorithm is a loop that includes steps 2-5. In every iteration, one voxel $\mathbf{m}$ is removed from the list of candidate voxels until we pass once through all voxels in the DW-MRI dataset. Hence the total number of iterations equals to the number of voxels in the input dataset. As a result, a cost value is calculated for every pixel in the cost map $\mathbf{C}$, which is the output of the algorithm. According to the definition and properties of the fiber cost (Sec.3.1) and geometric cost (Sec.3.2), the cost value will significantly increase outside the traced perpendicular fiber section. One can visualize the traced fiber section either by superimposing the cost map on the top of the corresponding DW-MRI dataset (see Fig. 4), by plotting the computed cost map as semi-transparent density map using volume rendering techniques, or finally by extracting the 3D surface model using contours (See Figs. 1, 6, and 8).

Since in our particular application we are interested in a specific subset of voxels that belong to the region of interest around the seed voxel $\mathbf{s}$, we can stop the main loop of the algorithm before covering the entire dataset, reducing significantly the computational cost/execution time. This can be implemented by introducing an additional condition to step 4 of the algorithm for filtering out the candidate voxels $\mathbf{v}$ in the neighborhood of $\mathbf{m}$ that correspond to $Cost(\mathbf{v}) > C_{threshold}$, where $C_{threshold}$ is a user-defined value. Obviously, for large threshold values the method becomes identical to the previous version of the algorithm, as described above, and the cost map is calculated for the entire dataset. Similarly, one can introduce stronger conditions in step 4, that refine further the set of candidate voxels $\mathbf{v}$ using separate thresholds for $Cost_f(\mathbf{v})$ and $Cost_g(\mathbf{v})$.

In our experimental results (Sec. 5) we test the robustness of the proposed algorithm using various values for $C_{threshold}$. In the next section we present an application of the perpendicular fiber tracking algorithm for fiber bundle analysis.

4 Fiber Bundle Analysis

The algorithm for perpendicular fiber tracking presented in Sec. 3 can be used for fiber bundle analysis in conjunction with traditional fiber tracking techniques. The goal is to estimate useful quantities along a fiber bundle that characterize its structure and topology. Our proposed method for fiber bundle analysis is summarized below.

Algorithm *Fiber_Bundle_Analysis*

Input: A seed voxel location $\mathbf{s}$. A field of fiber (or multi-fiber) orientations.
Output: An array of cost maps $\mathbf{C}_i$ and their statistical measurements.

1 Perform fiber tracking from the seed point $\mathbf{s}$ using any traditional fiber tracking method.

2 For every point $\mathbf{p}_i$ along the fiber perform perpendicular fiber tracking using the proposed method and setting $\mathbf{p}_i$ as the seed point.

3 For every computed cost map $\mathbf{C}_i$, estimate its area and average curvature and plot the results as functions along the fiber.

4 Fiber bundle segmentation step (optional): Use each voxel in every perpendicular fiber section as a seed point for fiber tracking and plot the results, i.e. the entire traced fiber bundle.

End *Fiber_Bundle_Analysis*

The area of each of the perpendicular fiber sections estimated by our algorithm can be approximated/computed as the number of voxels in the cost map that intersect the solution surface. For example the voxels in the middline of the cost map in Fig. 4 correspond to the solution surface, and hence they should be included in the calculation of the area of the perpendicular fiber section. Similarly, the average curvature of a perpendicular fiber section can be approximated by the average angle of the underlying

fiber orientation between adjacent voxels on the solution surface. The values of these quantities can be presented as one-dimensional plots showing how they vary along the fiber bundle (see Figs. 2, 5, 7, and 9).

Furthermore, the set of traced perpendicular fiber sections along a fiber bundle can be perceived as the segmentation of the fiber bundle. The entire segmented fiber bundle can be plotted in 3D as a stack of fiber bundle sections. The voxels in the segmented region can also be used as seed points for tracking the fibers within the entire fiber bundle, as shown in Figs. 6 and 8.

An implementation of the algorithms presented here is available in Matlab© through the website of Matlabcentral[1]. The proposed methods are demonstrated and validated in the next section using real and synthetic DW-MRI datasets.

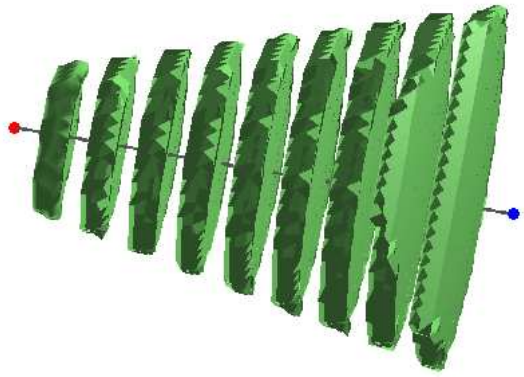

Figure 1 Results obtained by applying the proposed method for perpendicular fiber tracking to a synthetic DW-MRI dataset. The figure depicts the estimated fiber sections, which agree with the ground truth geometry of the synthetic fiber bundle.

5 Experimental Results

This section is organized into two subsections in which we present the experimental results obtained using synthetic data and real DW-MRI data from rat hippocampus.

5.1 Synthetic data experiments

In order to validate quantitatively the accuracy of the proposed algorithm, we synthesized a DW-MRI dataset by simulating the signal attenuation in the presense of restricted cylindrical diffusion model using the adaptive kernel implementation (5) of the realistic simulation model in (31). A set of 21 diffusion sensitizing gradient orientations was constructed using tessalations of the icosahedron on the unit sphere. The b-value was set to $1500s/mm^2$ and the matrix size of the simulated dataset was $60 \times 60 \times 60$. The synthetic dataset was created by simulating a single fiber bundle with straight parallel fibers within a conic section fiber bundle volume (Fig. 1). Due to this particular pre-defined fiber geometry, the ground truth curvature of the perpendicular fiber bundle sections was zero throughout the bundle and the ground truth area of the surfaces was linearly increasing.

After simulating the DW-MRI signal attenuation, we estimated the field of diffusion tensors using the method in (3). The principal eigenvector field of the diffusion tensors was provided as input to the proposed algorithm for fiber bundle analysis using perpendicular fiber tracking as presented in Sec. 3. The perpendicular fiber sections traced by our algorithm are shown in Fig. 1 (only 9 sections are displayed for clarity). The corresponding computed surface area and average curvature are plotted in Fig. 2. The obtained results conclusively demonstrate the accuracy of the proposed technique. The estimated values of both quantities for all the perpendicular sections match the ground truth values. The color of the plots goes gradually from red to blue to indicate the position along the fiber bundle as it

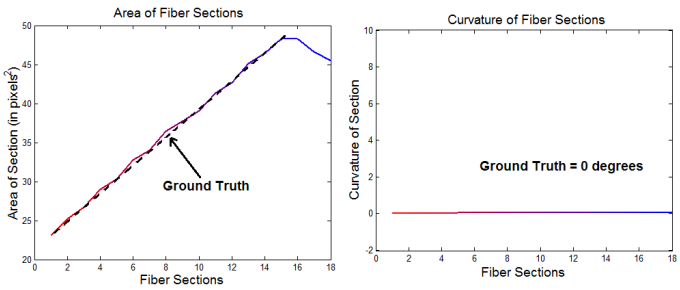

Figure 2 Comparison of the computed fiber section area and curvature with the ground truth values for all the estimated fiber sections (shown in Fig1).

is noted in Fig. 1 with the blue and red dot in the two ends of the bundle.

5.2 Real data experiments

After validating the algorithm on synthetic data, we then applied it on a real excised rat brain dataset to examine its clinical viability. Perpendicular fiber sections were traced in three different regions (*stratum radiatum, stratum lacunosum-moleculare and stratum oriens*) of rat hippocampus. The acquisition protocol included 21 diffusion-weighted image sets with a b-value of approximately $1250s/mm^2$ (6). A diffusion tensor field was estimated from the DW-MRI dataset using the method in (3). Fig. 3 shows the Fractional Anisotropy (FA) map of the dataset (top) and the corresponding FA color map using the square of the three components of the primary eigen vector field as the red, green, and blue color components (bottom).

In order to demonstrate the cost map estimated by our algorithm in the region of *stratum oriens*, we super impose the cost map over the FA map corresponding to the central slice of the 3D dataset. By observing the figure we can see that the midline of the cost map is alligned with geometric structures that are visible in the dataset.

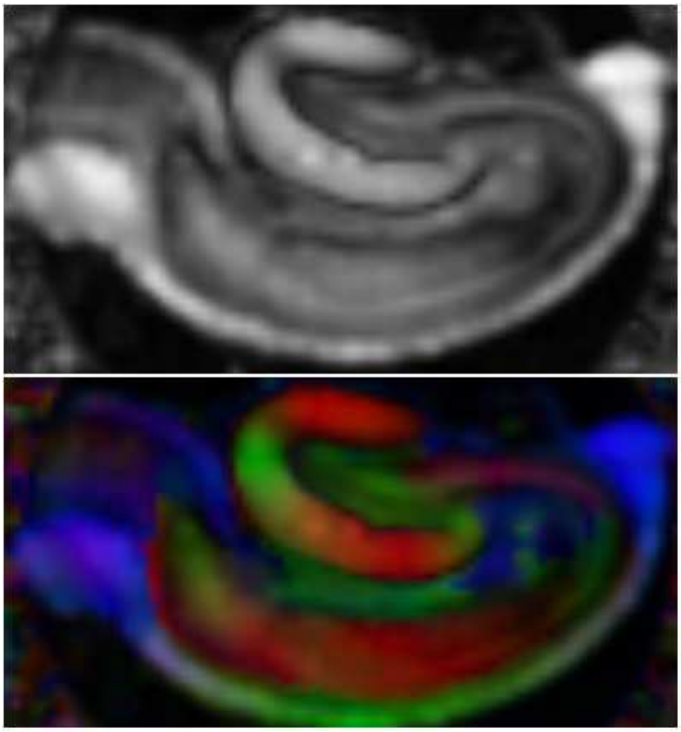

Figure 3 An image from the real DW-MRI dataset of rat hippocampus. The FA map is shown on the top, and the FA color map is shown on the bottom.

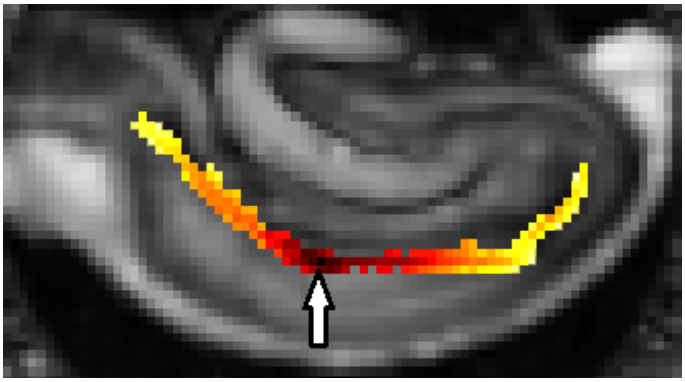

Figure 4 Visualization of the cost map computed by the proposed algorithm in the region of *stratum radiatum*. The arrow indicates the seed point.

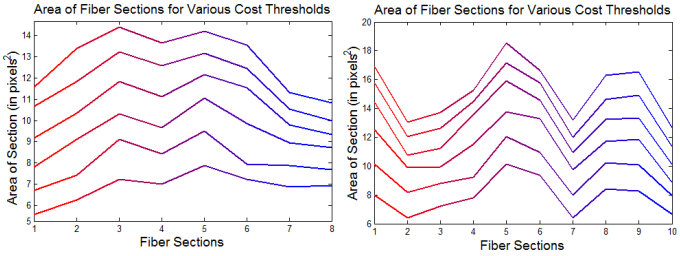

Figure 5 Demonstration of the robustness of the proposed algorithm tested using various threshold values. The figure shows that the shape and critical points of the plots remain the same for all test settings.

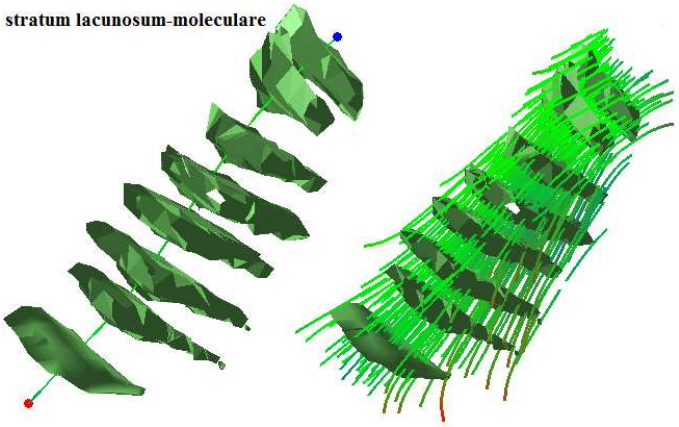

Figure 6 Results obtained by applying the proposed method for perpendicular fiber tracking to the rat hippocampal dataset 3. The figure depicts the estimated fiber sections (left) and the segmented bundle of fibers (left) in the region of *stratum lacunosum-moleculare*.

Furthermore, we demonstrate the robustness of the proposed algorithm using various threshold values $C_{threshold}$ ranging from 0.5 to 1.0 using 0.1 increments. The surface areas were computed from the corresponding cost maps for the regions of *stratum lacunosum-moleculare* and *stratum oriens* and are shown in Fig. 5. By observing the plots we can see that the structure, relative values, and critical points of the plotted lines do not change with the value of the threshold; only the absolute value changes, as expected. Therefore, these plots can be used as robust markers that characterize the structure of a fiber bundle. By comparing the plots in Fig. 5 obtained for the two hippocampal regions we can see that there are obvious structural differences, which agree with the traced perpendicular fiber sections shown in Figs. 6 and 8.

Figs. 6 and 8 show the perpendicular fiber sections traced by the proposed method in the regions of *stratum lacunosum-moleculare* and *stratum oriens* respectively. In each figure only 8 slices are shown for clarity. The figure also shows the segmented fiber bundle along with the fiber stream lines obtained by simple DTI-based fiber tracking (11) starting from every voxel in the fiber bundle. We chose these two particular hippocampal regions because they have significant

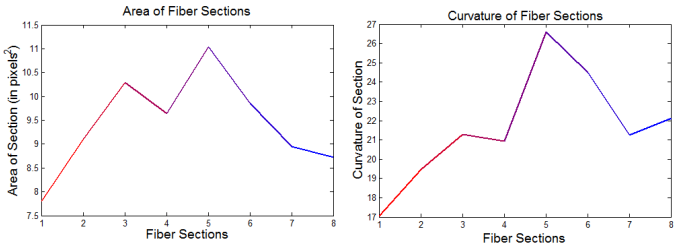

Figure 7 Plots of the estimated fiber section area and curvature values for the region of *stratum lacunosum-moleculare* (Fig. 6).

structural differences. The region of *stratum lacunosum-moleculare* follows a simple cylindrical fiber bundle model, while *stratum oriens* has the structure of a membrane wrapped around the hippocampus. Although the bundles have such structural and topological differences, the proposed algorithm correctly traced the perpendicular sections in both cases and both bundles were properly segmented.

Finally, Figs. 7 and 9 show the plots of the computed area and curvature of the estimated surfaces from both hippocampal regions. In both plots we used the threshold value $C_{threshold} = 0.7$, although its value does not play significant role, as it was discussed previously. It is known that quantitative comparison cannot be easily performed in real data due to the absense of ground truth. Nevertheless we can qualitatively evaluate the data by using knowledge on the structure of hippocampus (30) and observing that the estimated quantities follow the structural changes along the two bundles, as they are depicted in the 3D plots shown in Figs. 6 and 8.

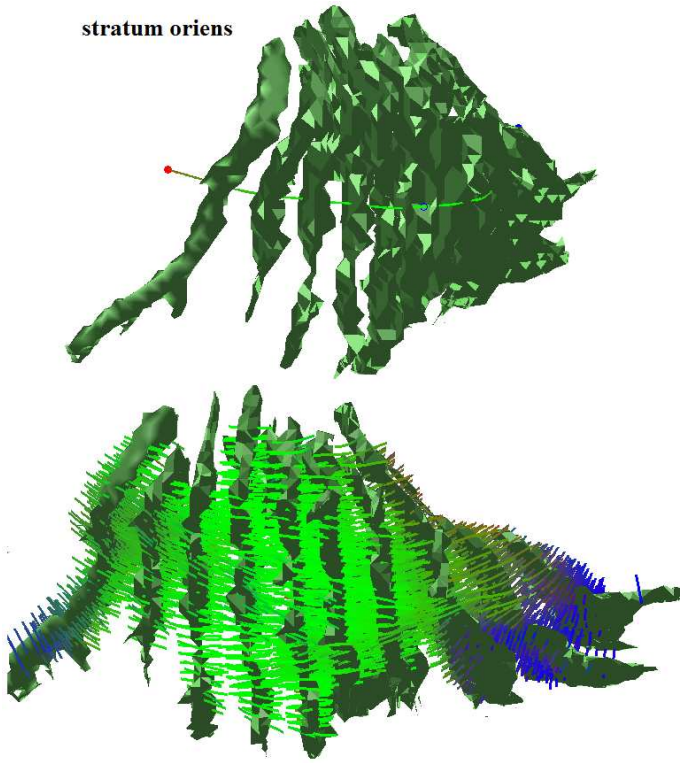

Figure 8 Plot of the estimated fiber sections in the region of *stratum oriens*. The segmented bundle of neural fibers is shown on the bottom.

6 Discussion and Conclusion

In conclusion, in this paper the idea of perpendicular fiber tracking was introduced, and an application for fiber bundle analysis was presented. The proposed algorithms were tested in synthetic, as well as real DW-MRI datsets. The validation experiments against the ground truth in the synthetic dataset demonstrated the efficiency and accuracy of our perpendicular fiber tracking technique.

The proposed method produces interactively (using a user-defined seed point) comprehensive statistics on area and curvature along fiber bundles with potential for real-time clinical use. The algorithm successfully performs perpendicular fiber tracking (in contrast to the existing techniques for tracking fiber along the principal direction) and can be employed for computing significant information on local fiber patterns of diffusion. The technique can be used as a tool for fiber bundle segmentation, for neural fiber analysis, and potentially as a biomarker for various brain diseases that involve change in white matter, including AD, PD, epilepsy, autism, and other *dementias*.

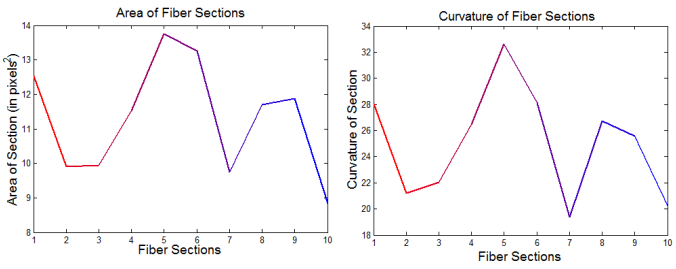

Figure 9 Plots of the estimated fiber section area and curvature values for the region of *stratum oriens* (Fig. 8).

In the future the method can be applied to diseased (AD, epilepsy, PD, cancer) brain data sets to detect patterns of changes in fiber geometry. Perpendicular tracking based on HARDI is expected to allow us to compute similar fiber bundle statistics for regions of fiber crossings and other complex fiber geometries and may also improve the analysis of small pathways and long tortuous pathways.

References

[1] I. Aganj, C. Lenglet, and G. Sapiro, *ODF reconstruction in Q-ball imaging with solid angle consideration*, in ISBI, 2009, pp. 1398–1401.

[2] A. W. Anderson, *Measurement of fiber orientation distributions using high angular resolution diffusion imaging*, MRM, 54 (2005), pp. 1194–1206.

[3] A. Barmpoutis, J. Ho, and B. C. Vemuri, *Approximating symmetric positive semi-definite tensors of even order*, SIAM Journal on Imaging Sciences, 5 (2012), pp. 434–464.

[4] A. Barmpoutis, M. S. Hwang, D. Howland, J. R. Forder, and B. C. Vemuri, *Regularized positive-definite fourth-order tensor field estimation from DW-MRI*, NeuroImage, 45 (2009), pp. 153–162.

[5] A. Barmpoutis, B. Jian, and B. C. Vemuri, *Adaptive kernels for multi-fiber reconstruction*, In LNCS 5636 (Springer) Proceedings of IPMI09: Information Processing in Medical Imaging, (2009), pp. 338–349.

[6] A. Barmpoutis, B. C. Vemuri, T. M. Shepherd, and J. R. Forder, *Tensor splines for interpolation and approximation of DT-MRI with applications to segmentation of isolated rat hippocampi*, TMI: Transactions on Medical Imaging, 26 (2007), pp. 1537–1546.

[7] A. Barmpoutis and J. Zhuo, *Diffusion kurtosis imaging: Robust estimation from dw-mri using homogeneous polynomials*, In Proceedings of ISBI11: IEEE International Symposium on Biomedical Imaging, (2011), pp. 262–265.

[8] P. J. Basser and et al, *Estimation of the effective self-diffusion tensor from the NMR spin echo.*, J. Magn. Reson. B, 103 (1994), pp. 247–254.

[9] P. J. Basser, J. Mattiello, and D. Lebihan, *Estimation of the Effective Self-Diffusion Tensor from the NMR Spin Echo.*, J. Magn. Reson. B, 103 (1994), pp. 247–254.

[10] P. J. Basser, J. Mattiello, and D. LeBihan, *Mr diffusion tensor spectroscopy and imaging*, Biophysical Journal, 66 (1994), pp. 259–267.

[11] P. J. Basser, S. Pajevic, C. Pierpaoli, J. Duda, and A. Aldroubi, *In vivo fiber tractography using DT-MRI data*, Magn. Reson. Med., 44 (2000), pp. 625–632.

[12] T. Behrens and et al, *Probabilistic tractography with multiple fibre orientations: What can we gain?*, NeuroImage, 34 (2007), pp. 144–155.

[13] U. Bozkaya and B. Acar, *Smt: Split and merge tractography for dt-mri*, In Medical Image Computing and Computer-Assisted Intervention - MICCAI, (2007), pp. 153–160.

[14] T. E. Conturo, N. F. Lori, T. S. Cull, E. Akbudak, A. Z. Snyder, J. S. Shimony, R. C. McKinstry, H. Burton, and M. E. Raichle, *Tracking neuronal fiber pathways in the living human brain*, Proc. Natl. Acad. Sci., 96 (1999), pp. 10422–10427.

[15] M. Descoteaux, E. Angelino, S. Fitzgibbons, and R. Deriche, *Regularized, fast and robust analytical q-ball imaging*, MRM, 58 (2007), pp. 497–510.

[16] P. Fillard, C. Poupon, and J. F. Mangin, *A novel global tractography algorithm based on an adaptive spin glass model*, Medical Image Computing and Computer-Assisted Intervention, 12 (2009), pp. 927–934.

[17] C. P. Hess and et al, *Q-ball reconstruction of multimodal fiber orientations using the spherical harmonic basis*, MRM, 56 (2006), pp. 104–117.

[18] J. H. Jensen, J. A. Helpern, A. Ramani, H. Lu, and K. Kaczynski, *Diffusional kurtosis imaging: The quantification of non-gaussian water diffusion by means of magnetic resonance imaging*, MRM, 53 (2005), pp. 1432–1440.

[19] B. Jian and et al, *A novel tensor distribution model for the diffusion weighted MR signal*, NeuroImage, 37 (2007), pp. 164–176.

[20] B. W. Kreher, I. Mader, and V. G. Kiselev, *Gibbs tracking: a novel approach for the reconstruction of neuronal pathways*, Magn Reson Med, 60 (2008), pp. 953–963.

[21] R. Kumar and et al, *Multi-fiber reconstruction from DW-MRI using a continuous mixture of von mises-fisher distributions*, in MMBIA, 2008.

[22] S. Mori, B. J. Crain, V. P. Chacko, and P. C. M. van Zijl, *Three-dimensional tracking of axonal projections in the brain by magnetic resonance imaging*, Ann. Neurol., 45 (1999), pp. 265–269.

[23] S. Mori and P. C. M. van Zijl, *Fiber tracking: principles and strategies - a technical review*, 2002.

[24] E. N. Mortensen and W. A. Barrett, *Interactive segmentation with intelligent scissors*, Graphical Models and Image Processing, 60 (1998), pp. 349–384.

[25] E. Ozarslan and T. H. Mareci, *Generalized diffusion tensor imaging and analytical relationships between DTI and HARDI.*, MRM, 50 (2003), pp. 955–965.

[26] L. Qi, D. Han, and E. X. Wu, *Principal invariants and inherent parameters of diffusion kurtosis tensors*, Journal of Mathematical Analysis and Applications, 349 (2009), pp. 165–180.

[27] A. Ramirez-Manzanares and et al, *Diffusion basis functions decomposition for estimating white matter intravoxel fiber geometry*, IEEE Trans. Med. Imaging, 26 (2007), pp. 1091–1102.

[28] Y. Rathi, O. Michailovich, S. Bouix, and M. Shenton, *Directional functions for orientation distribution estimation*, In: ISBI, (2008), pp. 927–930.

[29] M. Reisert, I. Mader, C. Anastasopoulos, M. Weigel, S. Schnell, and V. Kiselev, *Global fiber reconstruction becomes practical*, Neuroimage, 54 (2011), pp. 955–962.

[30] T. M. Shepherd and et al, *Structural insights from high-resolution diffusion tensor imaging and tractography of the isolated rat hippocampus*, NeuroImage, 32 (2006), pp. 1499–1509.

[31] O. Söderman and B. Jönsson, *Restricted diffusion in cylindirical geometry*, J. Magn. Reson. B, 117 (1995), pp. 94–97.

[32] E. O. Stejskal and J. E. Tanner, *Spin diffusion measurements: Spin echoes in the presence of a time-dependent field gradient,*, ournal of Chemical Physics, 42 (1965), pp. 288–292.

[33] J.-D. Tournier, F. Calamante, D. G. Gadian, and A. Connelly, *Direct estimation of the fiber orientation density function from diffusion-weighted MRI data using spherical deconvolution*, NeuroImage, 23 (2004), pp. 1176–1185.

[34] D. S. Tuch, *Q-ball imaging*, Magn. Reson. Med., 52 (2004), pp. 1358–1372.

Note

[1] An implementation of the algorithms presented here is available in Matlab© through the website of Matlab-central: http://www.mathworks.com/matlabcentral